



# Intraspinal Sensory Neurons Provide Powerful Inhibition to Motor Circuits Ensuring Postural Control during Locomotion

Jeffrey michael Hubbard, Urs lucas Böhm, Andrew Prendergast, Po-En brian Tseng, Morgan Newman, Caleb Stokes, Claire Wyart

## ► To cite this version:

Jeffrey michael Hubbard, Urs lucas Böhm, Andrew Prendergast, Po-En brian Tseng, Morgan Newman, et al.. Intraspinal Sensory Neurons Provide Powerful Inhibition to Motor Circuits Ensuring Postural Control during Locomotion. Current Biology - CB, 2016, 10.1016/j.cub.2016.08.026 . hal-01382762

**HAL Id: hal-01382762**

**<https://hal.sorbonne-universite.fr/hal-01382762>**

Submitted on 17 Oct 2016

**HAL** is a multi-disciplinary open access archive for the deposit and dissemination of scientific research documents, whether they are published or not. The documents may come from teaching and research institutions in France or abroad, or from public or private research centers.

L'archive ouverte pluridisciplinaire **HAL**, est destinée au dépôt et à la diffusion de documents scientifiques de niveau recherche, publiés ou non, émanant des établissements d'enseignement et de recherche français ou étrangers, des laboratoires publics ou privés.

# Title

Intraspinal sensory neurons provide powerful inhibition to motor circuits ensuring postural control during locomotion

# Authors

Jeffrey Michael Hubbard<sup>1-4</sup>, Urs Lucas Böhm<sup>1-4</sup>, Andrew Prendergast<sup>1-4</sup>, Po-En Brian Tseng<sup>1-4</sup>, Morgan Newman<sup>5</sup>, Caleb Stokes<sup>1-4</sup> and Claire Wyart<sup>1-4,#</sup>

# Affiliations

<sup>1</sup>Institut du Cerveau et de la Moelle épinière (ICM), Campus hospitalier universitaire de la Pitié-Salpêtrière, F-75013, Paris, France; <sup>2</sup>INSERM UMRS 1127, 75013 Paris, France ; <sup>3</sup>CNRS UMR 7225, 75005 Paris, France; <sup>4</sup>UPMC Univ. Paris 06, F-75005, Paris, France; <sup>5</sup> University of Adelaide, Adelaide, Australia.

# Corresponding author: Claire Wyart, ICM, Campus Hospitalier Pitié-Salpêtrière, 47 bld de l'hôpital, 75013 Paris, France. Phone: +33 1 57 27 43 10; Fax: + 33 1 57 27 40 46; [claire.wyart@icm-institute.org](mailto:claire.wyart@icm-institute.org)

# Summary

In the vertebrate spinal cord, cerebrospinal fluid-contacting neurons (CSF-cNs) are GABAergic neurons whose functions are only beginning to unfold. Recent evidence indicates that CSF-cNs detect local spinal bending and relay this mechanosensory feedback information to motor circuits. Yet many CSF-cN targets remain unknown. Using optogenetics, patterned illumination and *in vivo* electrophysiology, we show here that CSF-cNs provide somatic inhibition onto fast motor neurons and excitatory sensory interneurons involved in the escape circuit. Ventral CSF-cNs respond to spinal bending, including a longitudinal component, and induce large inhibitory postsynaptic currents (IPSCs) sufficient to silence spiking of their targets. Upon repetitive stimulation, these IPSCs promptly depress enabling the mechanosensory response to the first bend to be the most effective. When CSF-cNs



are silenced, postural control is compromised resulting in rollovers during escapes. Altogether our data demonstrates how GABAergic sensory neurons provide powerful inhibitory feedback onto the escape circuit to maintain balance during active locomotion.

## **Keywords**

spinal cord, connectome, CSF-cN, GABAergic sensory neuron, zebrafish, optogenetics, sensory-motor feedback, posture, escape behavior

## **Running title**

Ventral CSF-contacting neurons detect longitudinal contraction of the spinal cord and locally project onto elements of the escape circuit to control posture

## **Introduction**

Cerebrospinal fluid-contacting neurons (CSF-cNs) were first identified nearly a century ago and are highly conserved in the spinal cord, having been described in over 200 vertebrate species [1, 2]. Despite being a central element of the vertebrate spinal cord, the precise cellular connectivity and function of CSF-cNs is only recently beginning to be described [3-7]. CSF-cNs exhibit an apical dendritic extension bearing microvilli situated in the lumen of the central canal. These cells express the transient receptor potential channel TRPP3 (or Polycystic Kidney Disease 2-Like 1, PKD2L1) [8, 9], allowing them to respond to variations in pH and osmolarity in the CSF [4, 8]. Based on their anatomy, these cells have been proposed to detect flow or content of the CSF [10, 11].

Recently we demonstrated that dorsal CSF-cNs on either side of the central canal are activated by curvature of the spinal cord selectively on the side of bending in larval zebrafish [7]. We showed evidence that CSF-cNs modulate stereotyped behaviors in intact zebrafish thought to be driven by locomotor central pattern generators (CPGs), both for slow locomotion [5] as well as for fast locomotion during acoustic escapes [7]. However, precise cellular connections by which CSF-cNs modulate fast

locomotion have not been previously investigated. Escapes in fish are a stereotyped movement program that is typically triggered by the sequential activation of sensory neurons, leading to recruitment of the Mauthner cell in the hindbrain [12, 13] and finally the activation of spinal neurons including primary motor neurons. This induces a large C-bend on one side of the animal that is coincident with recruitment of commissural inhibitory glycinergic interneurons to silence motor output on the other side [14, 15]. The neurons that underlie locomotion are known to reside in the ventral spinal cord where CSF-cNs send most of their projections [3, 5, 11]. This places CSF-cNs in an optimal position to modulate the spinal escape circuit. To establish the postsynaptic targets of CSF-cNs within the spinal cord, we combined whole cell patch clamp recordings of putative targets with 2D light patterning and ChannelRhodopsin (ChR2) mediated activation of CSF-cNs in the zebrafish larva. We took advantage of transgenic lines labeling specific classes of spinal neurons in order to target the recordings to given cell types, whose identity was later confirmed by cell filling and morphological reconstruction.

Here we provide evidence that ventral CSF-cNs are recruited during spontaneous contraction of the animal involving a longitudinal bend. We show that these CSF-cNs innervate multiple components of the escape circuit, namely, a subset of primary motor neurons as well as a class of glutamatergic interneurons involved in sensory motor gating. We found that this connectivity with key elements of the escape circuit is specific since CSF-cNs did not project onto either glycinergic premotor interneurons or mechanosensory neurons involved in the escape response. Ventral CSF-cNs provide somatic, perisomatic and axon initial segment innervation onto primary motor neurons, reminiscent of basket-cell synapses. The innervation of the motor neuron pool by CSF-cNs is selective for caudal primary motor neurons referred to as CaP, which are involved in fast locomotion and postural control [16, 17]. The innervation of sensory interneurons is restricted to the initial segment and soma, with occasional axo-dendritic contacts. On both of these CSF-cN targets, ventral CSF-cNs induce a remarkably large and reliable inhibitory postsynaptic current (IPSC) with similar properties. Stimulus trains at moderate frequencies (10-

20Hz) rapidly induce short-term depression of the postsynaptic response. Spatially-restricted photoactivation of single CSF-cNs indicates that multiple CSF-cNs converge onto a given target. The convergence of inputs onto single primary motor neurons from ventral CSF-cNs provides strong GABAergic inhibition capable of efficiently silencing motor output. Furthermore, we show behaviorally that silencing CSF-cN output with botulinum toxin results in a defect in postural control during acoustically induced escapes responses.

Our findings demonstrate that an intraspinal GABAergic system actively senses spinal cord curvature during locomotion and constitutes a local sensory-motor loop that modulates posture during rapid movement.

## **Results**

### **Dorsal projections from ventral CSF-cNs innervate primary motor neurons**

In order to identify CSF-cN targets, we carefully investigated the morphology of their axonal projections. While a large density of CSF-cN axons project within the ventral portion of the spinal cord [5], some of the ventral CSF-cNs extend axonal projections dorsally, encircling large cell bodies (Figure 1A-C, 1E). This structure contained multiple large varicosities (Figure 1A, 1B) associated with putative presynaptic boutons labeled by Synaptophysin-GFP (Figure 1C). The position of these presynaptic structures suggested innervation of dorsal primary motor neurons (pMNs), which are recruited during escapes and fast swimming in zebrafish larvae [17]. We screened different transgenic cell lines labeling specific cell types in the zebrafish spinal cord and identified the anatomical contact of CSF-cNs to caudally-located dorsal primary motor neurons (Figure 1E), referred to as CaP [18].

### **Selective connectivity onto primary motor neurons involved in fast locomotion and postural control**

To test the functional connectivity of CSF-cNs to primary motor neurons, we optically

activated CSF-cNs expressing ChR2 while recording from the cell body surrounded by presynaptic boutons (Figure 1D). Cells whose soma were encircled by the CSF-cN basket structure correspond to CaP primary motor neurons as shown by their characteristic morphology after dye filling (Figure 1E), their input resistance, and their sustained firing of action potentials at high frequency (Figure 1F). The morphology of the axonal projection suggests that individual CSF-cNs innervate multiple CaP motor neurons along the rostro-caudal axis (Figure 1E). In our conditions, a 5 ms light pulse typically induces a single spike in CSF-cNs expressing ChR2-mCherry (see [5]). Following the optical activation of CSF-cNs, we recorded large IPSCs in CaP motor neurons occurring without failure (34 out of 34 CaP motor neurons recorded). These IPSCs were abolished by bath application of the GABA<sub>A</sub> receptor antagonist gabazine (Figure 1G, 1H). The light-induced current-voltage relationship showed that the IPSCs reversed around - 53 mV, close to the calculated reversal potential of chloride in our conditions ( $E_{Cl} = - 51$  mV, Figure 1I, 1J). The timing and kinetics of the light-induced IPSCs were consistent with monosynaptic currents mediated by GABA<sub>A</sub> receptors (Figure 1K-N). These data indicate that CaP motor neurons are one major target of CSF-cNs.

### **Other motor neurons are minimally innervated by CSF-cNs**

Given the significant innervation pattern observed for CaP motor neurons, we proceeded to determine whether other motor neurons (both primary and secondary) receive synaptic input from CSF-cNs. Targeted whole cell recordings of primary and secondary motor neurons were performed in *Tg(parg<sup>mnet2</sup>-GFP)* transgenic fish (Figure 2A). As shown previously, CaP motor neurons were distinguished based on soma location within the segment and the characteristic basket-like synaptic contacts from CSF-cNs (Figure 1A, 1B, 1E and Figure 2A, CaP motor neurons indicated by "C" in magnified images). Responses for non-CaP primary motor neurons (Figure 2A magnified boxes, indicated by arrows) following ChR2-mediated activation of CSF-cNs fell into three classes (Figure 2B1-B3). Only one non-CaP primary motor neuron out of 17 recorded showed IPSCs comparable to responses observed in CaP motor neuron recordings (Figure 2B1, lower panel). In 11 of 17 non-CaP primary motor

neurons the postsynaptic responses were very small (< 5 pA, Figure 2B2, lower panel) and in the remaining 5 non-CaP primary motor neurons no IPSCs were observed (Figure 2B3, lower panel). The majority of IPSCs observed in non-CaP primary motor neurons were of small amplitude (< 5 pA, Figure 2C). All but two of the events greater than 10 pA were observed in trials from a single neuron (Figure B1), suggesting that CSF-cN innervation of primary motor neurons is overwhelmingly restricted to CaP motor neurons. Secondary motor neurons were also tested for CSF-cN connectivity and were targeted based on fluorescence, ventral location and small soma size in the *Tg(parg<sup>mnet2</sup>-GFP)* transgenic line (Figure 2A magnified boxes, indicated by arrowheads). Secondary motor neurons showed typical bursting action potential firing patterns (see example in Figure 2D), however CSF-cN activation with 5 ms blue light pulses never produced IPSCs in secondary motor neurons in 10 of 10 cells recorded (Figure 2E, three secondary motor neuron examples shown). CSF-cNs therefore form very specific contacts within the motor pool onto CaP motor neurons.

### **Optogenetic-mediated mapping reveals connectivity onto sensory interneurons**

We noted that some of the CSF-cN axons project to the dorsal spinal cord, suggesting they target other spinal neurons. We hypothesized that they might target sensory interneurons in this population and tested a subtype of glutamatergic interneuron (called CoPA), known to be involved in sensory-motor gating and recruitment of motor neurons in the contralateral spinal cord [19, 20]. By selectively labeling CoPA interneurons in the *Tg(tbx16-GFP)* line [21], we observed that some CSF-cN varicosities were located on the CoPA soma (Figure 3A1, 3A2) and axon initial segment (Figure 3A1-A4). Interestingly, we noted that the morphology of CSF-cN axons suggests that an individual CSF-cN in contact with CaP (forming the basket-like synapse) may also diverge onto the adjacent CoPA dendrite (Figure 3A3, 3A4). We performed targeted whole cell patch clamp recordings (Figure 3B) and simultaneous photostimulation of CSF-cNs and found evidence of monosynaptic connections onto CoPA interneurons (Figure 3C). CoPA IPSCs were large and did not fail (8 out of 8 cells, Figure 3C). The IPSCs recorded in CoPA showed properties typical of GABA<sub>A</sub> mediated currents, similar to the IPSCs recorded in CaP motor

neurons (Figure 3D-G). However, IPSC amplitudes tended to be larger for CoPA sensory interneurons than those observed in CaP motor neurons (Figure 3H).

### **Convergence of inputs from multiple CSF-cNs onto individual targets**

We took advantage of a 2D light patterning approach [3, 22] to activate specific ChR2-expressing cells within the zebrafish spinal cord in order to test the connectivity of individual CSF-cNs onto CaP and CoPA targets (Figure 4). We used a custom-built illumination setup based on a Digital Mirror Device (Figure 4A) to pattern the stimulation light to spatially restricted targets (Figure 4B, 4C). The light stimulation was effective in triggering an IPSC only when it was directed onto the soma or occasionally on the initial segment of CSF-cNs (Figure 4D) but not on the rest of the axonal projection, including the varicosities within the basket structure surrounding the soma of the recorded cell (Figure 4D). The amplitude of IPSCs tended to decrease as a function of distance between the presynaptic CSF-cN and its target, with connections emanating from CSF-cNs less than three segments away from the target producing the largest responses (Figure 4E). Our data also shows that multiple CSF-cNs often innervate the same target neuron, either the CaP motor neuron (Figure 4D, 4F and 4G) or CoPA interneuron (Figure 4H), indicating a high degree of convergence from CSF-cNs onto their targets.

### **Neither commissural glycinergic neurons nor mechanosensory neurons involved in the escape circuit receive inputs from CSF-cNs**

We next sought to address whether the functional connectivity of CSF-cNs was specific to the glutamatergic interneurons and motor neurons of the escape circuit or whether they exert a distributed modulation impacting all elements of the escape pathway. We tested whether CSF-cNs project on the contralaterally-projecting glycinergic neurons, referred to as CoLo cells, involved in silencing activity on the contralateral side during the initial tail bends of the escape response ([15], Figure 5A-C). Targeted patch clamp recordings of CoLos using the *Tg(Tol-056-GFP)* transgenic line ([15], Figure 5A) showed no light-induced IPSCs in 13 out of 13 CoLos recorded (Figure 5B, 5C three examples shown). We also tested the connectivity onto

mechanosensory Rohon-Beard neurons that are well upstream of the escape circuit. Anatomical analysis of Rohon-Beard neurons and CSF-cNs in the *Tg(p2rx3.2:GFP ; pkd2l1:gal4 ; UAS:ChR2-mCherry)* triple transgenic larvae showed no overlap of CSF-cN axons onto the Rohon-Beard soma or axons ([23], Figure 5D). Whole cell recordings of Rohon-Beard neurons were performed to rule out functional connectivity to CSF-cNs (Figure 5E, 5F). IPSCs in Rohon-Beard neurons were never observed following ChR2-mediated activation of CSF-cNs with 5 ms light pulses (Figure 5F, n = 10, three examples shown). Taken together our data establishes a map of CSF-cN innervation onto specific elements of the escape circuit. CSF-cNs create extensive synaptic contacts specifically onto CaP primary motor neurons and CoPA glutamatergic sensory interneurons with minimal projections onto other primary motor neurons, and an exclusion of projections on secondary motor neurons, CoLo glycinergic commissural interneurons and the Rohon-Beard mechanosensory neurons.

#### **CSF-cN synapses onto targets of the escape circuit show strong short term depression**

Common features of CSF-cN mediated IPSCs recorded from primary motor and sensory interneurons include their high reliability and large amplitude (Figure 6A1-A3). Since CSF-cNs are recruited by spinal curvature during active locomotion [7], we tested whether these synapses showed short term plasticity when stimulated at higher frequencies corresponding to larval swimming (10-20Hz, Figure 6C, 6D). While 1 Hz stimulation induced moderate short-term depression following 10 light pulses (Figure 6B1-B3), raising the stimulation frequency to 10 and 20 Hz led to an incremental increase in short term synaptic depression (Figure 6C1-C3, 6D1-D3).

#### **A single CSF-cN action potential leads to prompt silencing of spiking in CSF-cN targets within the escape circuit**

Although we showed that CSF-cN firing causes a large and reliable chloride conductance in CaP motor neurons and CoPA sensory interneurons, the impact of this modulation on the output of the CPG, namely motor neuron activity, was

unclear. It has been suggested that an immature chloride gradient in the larval spinal cord could lead GABAergic input to be depolarizing in postsynaptic neurons [24]. We therefore tested how CSF-cNs modulated the spiking of their motor neuron targets by recording CaP motor neurons in cell-attached mode to preserve the chloride gradient in the postsynaptic neuron. A large voltage step induced high frequency firing in CaP motor neurons in this configuration (Figure 7A, 7B). A 5 ms light pulse (producing a single large IPSC) was sufficient to transiently silence the spiking of CaP motor neurons (Figure 7B, 7C). Quantification of the maximum interspike interval (ISI) for control trials and trials where a 5 ms light pulse activated CSF-cNs showed a significant increase after the light pulse in all cells tested (ISI control =  $9.10 \text{ ms} \pm 3.04 \text{ ms}$ , ISI light  $26.69 \text{ ms} \pm 10.55 \text{ ms}$ ,  $n = 4$ ), confirming the inhibitory nature of the GABAergic IPSCs from CSF-cNs onto their targets (Figure 7D).

#### **CSF-cNs are mechanosensory cells that control balance during fast locomotion**

We monitored CSF-cN activity using the calcium genetically-encoded indicator GCaMP3 combined with the position marker mCherry in unparalyzed larvae, which were mounted on their side and embedded in agarose. In these conditions, we found that ventral CSF-cNs are recruited during spontaneous longitudinal contractions (Figure S1 and Movie S1). Imaging and functional mapping experiments suggest that only ventral CSF-cNs, not dorsal CSF-cNs, innervate CaP primary motor neurons involved in postural control (Figure 1E and Figure 4D, 4F and 4G). From these results we hypothesized that ventral CSF-cNs could act as a mechanosensory system detecting longitudinal spinal bending and subsequently provide inhibitory tone to CaP motor neurons. We tested this hypothesis by analyzing the behavior of animals in which CSF-cN synapses were silenced by botulinum toxin [7]. We reanalyzed the dataset from Böhm, et al. and rollover events were scored by a blinded observer. We determined a roll ratio for each fish (number of trials the fish rolled/the number of trials the fish responded to the acoustic stimulus) and found that rollovers occurred twice as often in animals expressing botulinum toxin in CSF-cNs compared to control siblings (Figure 7E, 7F and Movies S2 and S3). This result indicates that CSF-cNs contribute to maintaining balance during active locomotion.



## Discussion

### **Selective inhibition from GABAergic sensory neurons onto sensory interneurons and motor neurons of the escape circuit**

Our work demonstrates a strong and selective connection from CSF-cNs onto primary motor neurons and glutamatergic sensory interneurons (CaP and CoPA respectively). This connectivity appears specific within the escape circuit of the zebrafish spinal cord, as CSF-cNs avoid synaptic contacts to secondary motor neurons, mechanosensory neurons and glycinergic premotor interneurons which are involved in escapes. CSF-cN input to motor neurons is mainly limited to the primary motor neuron, CaP, while other primary motor neurons generally receive little to no synaptic input. The specificity of the CSF-cN synapse onto CaP motor neurons suggests that these motor neurons may play a specialized role that differs from other primary motor neurons. CaP motor neurons are the first motor neurons to extend from the spinal cord to the skeletal muscle in the developing embryo [18]. Primary motor neurons (CaP, MiP, and the two RoPs) innervate distinct territories of axial, fast skeletal muscle fibers. Of the primary motor neurons, CaP innervates the largest field of fast skeletal muscle, covering approximately 2/3rds of the ventral fibers. The differential activation of primary motor neurons is thought to induce body torque and therefore a change in vertical trajectory [16]. Beyond their importance in fast locomotion and the escape response, CaP motor neurons most likely play a role in maintaining postural control. In this study, we observe that CSF-cNs project selectively onto CaP motor neurons, and that the silencing of CSF-cNs leads to a balance defect causing larvae to tip and roll over during acoustically induced escape responses. This observation suggests that inhibition to CaP motor neurons by CSF-cNs plays a critical role in the control of posture during fast swimming. Yet, we cannot exclude that other putative targets of CSF-cNs contribute to this effect as well.

### **Physiology of CSF-cN synapses onto their targets within the escape circuit**

The somatic and axonic innervation of CSF-cNs onto CaP motor neurons and CoPA

interneurons is enhanced by the convergence of inputs from multiple CSF-cNs onto one target neuron. This convergence is reminiscent of the projection from basket cells onto pyramidal neurons [25-28], and is associated with large reliable IPSCs. The CSF-cN mediated inhibition from a single spike is efficient enough to transiently silence postsynaptic targets within the escape circuit. At higher stimulation frequencies, synapses of CSF-cNs onto their targets rapidly depress. In direct recordings from CSF-cNs in the cell-attached configuration, optogenetically-mediated activation of CSF-cNs has been confirmed up to 25Hz without action potential failures. We therefore believe that the observed plasticity most likely reflects a presynaptic mechanism consistent with other high release probability synapses that undergo short-term depression rather than failure to optogenetically elicit spiking in CSF-cNs. Remarkably, the short-term depression occurs at frequencies that closely match the naturally occurring tail beat frequencies of zebrafish larvae. A result of this property is that within this range of CSF-cN firing frequencies, the first IPSC is the most effective at modulating the spiking of motor and sensory interneuron targets. This feature suggests a homeostatic function for the feedback inhibition provided by CSF-cNs: large motor neurons triggering the massive muscle contractions during the C-bend also recruit GABAergic sensory neurons that rapidly silence them.

The physiology of CSF-cN synapses onto elements of the fast escape circuit shown here is remarkably different from their modulation of the slow swimming circuit [5]. The connections from CSF-cNs onto MCoD glutamatergic premotor interneurons produce small amplitude IPSCs that are subject to failures and facilitate during repetitive stimulation [5]. In contrast, the projections of CSF-cNs onto both CaP and CoPA targets within the escape circuit are large, show no failure and rapidly depress over time. During repetitive contractions when the animal swims at high speed, this GABAergic sensory-motor pathway may therefore promptly silence motor neurons and interneurons involved in the initial phase of the escape, enabling a tight control on spike timing of motor neurons and a rapid transition from fast to slow swimming frequencies [29].

## Relevance to physiology and postural control

As indicated by anatomy [3, 5, 30-33], we demonstrate, using physiology and optogenetics, that the GABAergic sensory feedback provided on the escape circuit is local and intraspinal, never reaching targets more than five segments away in the larval stage. This GABAergic pathway can therefore locally tune the excitability of components of the escape in the spinal cord, without affecting the activity of reticulospinal neurons in the hindbrain.

Fast escapes in zebrafish larvae are highly regulated both in terms of lateral displacement as well as vertical elevation [34], so that larvae do not perform spiral trajectories as seen in *Xenopus* tadpoles [35]. Control of posture most certainly involves visual and vestibular feedback relayed by reticulospinal neurons down the spinal cord in order to optimally activate primary motor neurons [36]. Here we describe a local sensory-motor pathway for regulating posture situated within the spinal cord, a concept which had to our knowledge has only been described in birds where balance is stabilized by the vestibular organ during flight and by the lumbosacral system during walking [37]. By genetically targeting the optimized botulinum toxin to selectively block synaptic release from CSF-cNs, we observed a balance defect in BoTx fish compared to control siblings not expressing the toxin. Animals with CSF-cN neurotransmission silenced were twice as likely as their wild type siblings to tip and roll over during an acoustically induced escape response. In addition, we show that ventral CSF-cNs project onto CaP motor neurons and are physiologically activated during longitudinal contractions, which is not the case in differential left or right bending of the tail [7]. These results point to an asymmetrical proprioceptive function for CSF-cNs, whereby dorsal CSF-cNs respond to left or right horizontal bending while ventral CSF-cNs respond to longitudinal bending of the spinal cord. CSF-cNs would therefore provide mechano-sensory feedback during locomotion to inhibit motor output through the specific connectivity to the CaP motor neuron and excitatory interneurons such as CoPA and MCoDs. CSF-cNs therefore may constitute a mechanosensory system within the spinal cord, which

provides important proprioceptive feedback to coordinate locomotion and balance. The CSF-cNs may themselves be modulated by reticulospinal neurons or vestibulospinal pathways involved in the control of posture. This will be the focus of future investigations as descending inputs were severed by decapitation prior to testing intraspinal CSF-cN connectivity in this study.

## **Experimental Procedures**

### *Animal care and transgenics used*

Animal handling and procedures were validated by the Institut du Cerveau et de la Moelle épinière (ICM, Paris) and the French National Ethics Committee (Comité National de Réflexion Éthique sur l'Expérimentation Animale- Ce5/2011/056) in agreement with the European Union legislation. Adults were reared at a maximal density of 8 animals per liter in a 14/10 (light/dark) cycle environment. Fish were fed live artemia twice a day and feeding regime was supplemented with solid extracts matching the developmental stage (ZM Systems, UK). Larvae were raised at 28.5°C with a 14/10 (light/dark) light cycle. Experiments were performed at room temperature (22-25°C) on 3 to 7 dpf larvae. All transgenic lines used here are detailed in Suppl. Table S1. We injected the UAS:synaptophysin-GFP [38] DNA construct at 60 ng/μl into *Tg(pkcd2l1:gal4;UAS:Chr2-mCherry)* single cell-stage embryos.

### *Electrophysiology*

3-7dpf zebrafish larvae were decapitated and pinned to a Sylgard coated recording chamber (Sylgard 184, Dow Corning, Midland, MI, USA) through the notochord with electrolytically sharpened tungsten pins. The skin was removed and the specimen was bathed briefly in a 10% formamide solution and subsequently washed in bath recording solution to eliminate spontaneous muscle twitching. The dura was exposed by suctioning away dorsal muscle fibers with a glass pipette. Typically 3-7 segments of dorsal muscle were removed. Recording electrodes were fashioned from capillary glass (1.5 mm O.D., 1.1 ID, WPI, Sarasota, FL, USA) with a horizontal

puller (P1000, Sutter Instruments, Novato, CA). Electrode resistances were 10-16 M $\Omega$ . Positive pressure (65mm Hg) was applied to the recording electrode via a pneumatic transducer (Fluke Biomedical DPM1B, Everett, WA). Once the electrode was driven through the dura in order to approach neurons targeted for patch experiments, the positive pressure was reduced to 35mm Hg [39]. Cells were chosen based on their soma location matching the axonal projections of CSF-cNs expressing ChR2-mCherry and the expression of GFP in the transgenic lines used (Table S1). External bath recording solution contained the following (in mM), 134 NaCl, 2.9 KCl, 2.1 CaCl<sub>2</sub>-H<sub>2</sub>O, 1.2 MgCl<sub>2</sub>, 10 Glucose, 10 HEPES with pH adjusted to 7.4, and osmolarity to 290 mOsm. Spinal neuron internal solution contained the following (in mM), 115 K-Gluconate, 15 KCl, 2 MgCl<sub>2</sub>, 0.5 EGTA, 4 Mg-ATP, 10 HEPES pH 7.2, 290 mOsm. All reagents were obtained from Sigma-Aldrich (St. Louis, MO, USA) unless otherwise noted. Patch electrodes contained 40 $\mu$ M Alexa Fluor 488 or 594 hydrazide (Life Technologies Ltd., Paisley, UK). Physiological recordings were made with an Axopatch 700B amplifier and digitized with a Digidata 1440A (Molecular Devices, Fremont, CA, USA). pClamp software was used to acquire electrophysiological data at a sampling rate of 50 kHz and low pass filtered at 2.2 kHz. Data were analyzed with Clampfit (Molecular Devices, Fremont, CA, USA), Igor Pro 6.34 (WaveMetrics, Lake Oswego, OR), Excel 2010 (Microsoft, Redmond, WA, USA), and Matlab (Mathworks, Natick, MA, USA). Summary data are presented as average  $\pm$  SEM.

### *Confocal Imaging*

For imaging, larvae were prepared as described for physiological recordings. Confocal images were acquired with an Evolve 10 MHz Digital Monochrome Camera EM-CCD camera (Photometrics, Tucson, AZ, USA) using a Yokogawa X1 spinning disk (Yokogawa, Tokyo, Japan) mounted to an upright widefield microscope (Axio Examiner Z1, Zeiss, Germany) equipped with 20X, 40X, 63X water dipping objectives. Laser lines used here were a 50mW 488nm laser for imaging GFP and a 50 mW 561 nm laser for imaging mCherry. Z stacks were taken at 0.5  $\mu$ m step size. Data was acquired using SlideBook 6 image acquisition software (3i, Denver, CO, USA). Images were assembled with ImageJ (NIH, Bethesda, MD),

407 Adobe Photoshop and Illustrator CS6 (Adobe Systems Incorporated, San Jose, CA).

#### 408 *2D Light patterning using a DMD*

409 To generate the patterned illumination we used a DLP discovery kit including a 0.7"  
410 digital mirror device and software API (Vialux, Germany). The DMD was imaged via a  
411 telescope ( $f = 80$  mm and  $f = 40$  mm, Thorlabs, Newton, NJ, USA) onto the back  
412 focal plane of the epifluorescence light path of an upright widefield microscope (Axio  
413 Examiner D1, Zeiss, Germany). The DMD light path was combined with the  
414 epifluorescence light source via a 30% reflection 70% transmission beamsplitter (AHF,  
415 Germany) to allow the patterned and epifluorescence illumination through the same  
416 path. As a light source for the patterned illumination we used an ultra-high power  
417 white Light Emitting Device (LED, Prizmatix, Israel). The LED was coupled into the  
418 light path of the Digital Mirror Device (DMD) via a total internal reflection (TIR) prism  
419 (Lida optical and electronic, China). For fluorescent imaging and target cell selection  
420 the microscope was equipped with an EM-CCD camera (ImageEM, Hamamatsu,  
421 Japan). Integrated software control of the DMD and the camera was done via custom  
422 scripts in LabView (National Instruments, Austin, TX) and Matlab (Mathworks, Natick,  
423 MA). The Matlab code was partly based on Zhu et al., 2012 [40].

#### 424 *Behavior setup and analysis*

425 Behavior setup was previously described [7]. Each larva was subjected to five trials  
426 and rolling behavior was assessed for each trial. The roll ratio was calculated as the  
427 number of trials the animal rolled during an escape divided by the number of trials  
428 the animal attempted an escape. Roll ratio for BoTxBLC-GFP+ fish and control  
429 siblings are presented as average  $\pm$  SEM. Larvae were screened for GFP fluorescence  
430 to establish BoTx positive and BoTx negative siblings prior to data acquisition and  
431 the experimenter was blinded to genotype prior to assessment of the rolling  
432 behavior.

433

## Author Contributions

Conceptualization, J.M.H., C.S. and C.W.; Methodology, J.M.H., U.L.B., A.P., P.B.T., C.S. and C.W.; Software, U.L.B.; Formal Analysis, J.M.H. and C.W.; Investigation, J.M.H.; Resources, M.N. and C.W.; Writing, J.M.H. and C.W. who received inputs from all authors; Visualization, J.M.H.; Funding Acquisition, J.M.H., U.B., A.P. and C.W.; Supervision, C.W.

## Acknowledgements

We thank Prof. Shin-Ichi Higashijima, Prof. Darius Balciunas, Prof. David McLean, Prof. Mark Voigt and Prof. Herwig Baier for kindly sharing transgenic lines. We thank Natalia Maties, Bodgan Buzurin and Sophie Nunes Figueiredo from the ICM zebrafish facility for fish care. This work received support from the ICM, Ecole des Neurosciences de Paris (ENP), the Fondation Bettencourt-Schueller, the City of Paris Emergence program, the Atip/Avenir program from CNRS and Inserm, Marie Curie Actions (International Reintegration Grant, IRG #227200), the ERC starting grant Optoloco (#311673), the Philippe Foundation, and the Wings for Life foundation (Contract #WFL-FR-009/14, Project #91). The authors declare no conflict of interest.

## References

1. Kolmer, W. (1921). Das "Sagittalorgan" der Wirbeltiere. In *Z Anat Entwicklungs*, pp. 652–717.
2. Agduhr, E. (1922). Über ein Zentrales Sinnesorgan beiden Vertebraten. In *Z Anat Entwicklungs*, pp. 223–360.
3. Wyart, C., Del Bene, F., Warp, E., Scott, E.K., Trauner, D., Baier, H., and Isacoff, E.Y. (2009). Optogenetic dissection of a behavioural module in the vertebrate spinal cord. *Nature* 461, 407–410.

- 460 4. Orts-Del'immagine, A., Wanaverbecq, N., Tardivel, C., Tillement, V., Dallaporta, M.,  
461 and Trouslard, J. (2012). Properties of subependymal cerebrospinal fluid contacting  
462 neurones in the dorsal vagal complex of the mouse brainstem. *J. Physiol.* 590, 3719-  
463 3741.
- 464 5. Fidelin, K., Djenoune, L., Stokes, C., Prendergast, A., Gomez, J., Baradel, A., Del  
465 Bene, F., and Wyart, C. (2015). State-Dependent Modulation of Locomotion by  
466 GABAergic Spinal Sensory Neurons. *Curr. Biol.* 25, 3035-47.
- 467 6. Jalalvand, E., Robertson, B., Wallen, P., and Grillner, S. (2016). Ciliated neurons  
468 lining the central canal sense both fluid movement and pH through ASIC3. *Nature*  
469 *Communications* 7, 10002.
- 470 7. Böhm, U.L., Prendergast, A., Djenoune, L., Nunes Figueiredo, S., Gomez, J., Stokes,  
471 C., Kaiser, S., Suster, M., Kawakami, K., Charpentier, M., Concordet, J.P., Rio, J.P., Del  
472 Bene, F., and Wyart, C. (2016). CSF-contacting neurons regulate locomotion by  
473 relaying mechanical stimuli to spinal circuits. *Nature Communications* 7, 10866.
- 474 8. Huang, A.L., Chen, X., Hoon, M.A., Chandrashekar, J., Guo, W., Trankner, D., Ryba,  
475 N.J., and Zuker, C.S. (2006). The cells and logic for mammalian sour taste detection.  
476 *Nature* 442, 934-938.
- 477 9. Djenoune, L., Khabou, H., Joubert, F., Quan, F.B., Nunes Figueiredo, S., Bodineau,  
478 L., Del Bene, F., Burckle, C., Tostivint, H., and Wyart, C. (2014). Investigation of spinal  
479 cerebrospinal fluid-contacting neurons expressing PKD2L1: evidence for a conserved  
480 system from fish to primates. *Front. Neuroanat.* 8, 26.
- 481 10. Vigh, B., and Vigh-Teichmann, I. (1998). Actual problems of the cerebrospinal  
482 fluid-contacting neurons. *Microsc. Res. Tech.* 41, 57-83.
- 483 11. Stoeckel, M.E., Uhl-Bronner, S., Hugel, S., Veinante, P., Klein, M.J., Mutterer, J.,  
484 Freund-Mercier, M.J., and Schlichter, R. (2003). Cerebrospinal fluid-contacting neurons  
485 in the rat spinal cord, a gamma-aminobutyric acidergic system expressing the P2X2  
486 subunit of purinergic receptors, PSA-NCAM, and GAP-43 immunoreactivities: light



487 and electron microscopic study. *J. Comp. Neurol.* 457, 159-174.

488 12. Fetcho, J.R. (1991). Spinal network of the Mauthner cell. *Brain Behav. Evol.* 37,  
489 298-316.

490 13. Lacoste, A.M., Schoppik, D., Robson, D.N., Haesemeyer, M., Portugues, R., Li, J.M.,  
491 Randlett, O., Wee, C.L., Engert, F., and Schier, A.F. (2015). A convergent and essential  
492 interneuron pathway for Mauthner-cell-mediated escapes. *Curr. Biol.* 25, 1526-1534.

493 14. Fetcho, J.R., and Faber, D.S. (1988). Identification of motoneurons and  
494 interneurons in the spinal network for escapes initiated by the mauthner cell in  
495 goldfish. *J. Neurosci.* 8, 4192-4213.

496 15. Satou, C., Kimura, Y., Kohashi, T., Horikawa, K., Takeda, H., Oda, Y., and  
497 Higashijima, S. (2009). Functional role of a specialized class of spinal commissural  
498 inhibitory neurons during fast escapes in zebrafish. *J. Neurosci.* 29, 6780-6793.

499 16. Bagnall, M.W., and McLean, D.L. (2014). Modular organization of axial  
500 microcircuits in zebrafish. *Science* 343, 197-200.

501 17. Menelaou, E., and McLean, D.L. (2012). A gradient in endogenous rhythmicity  
502 and oscillatory drive matches recruitment order in an axial motor pool. *J. Neurosci.*  
503 32, 10925-10939.

504 18. Myers, P.Z., Eisen, J.S., and Westerfield, M. (1986). Development and axonal  
505 outgrowth of identified motoneurons in the zebrafish. *J. Neurosci.* 6, 2278-2289.

506 19. Pietri, T., Manalo, E., Ryan, J., Saint-Amant, L., and Washbourne, P. (2009).  
507 Glutamate drives the touch response through a rostral loop in the spinal cord of  
508 zebrafish embryos. *Dev. Neurobiol.* 69, 780-795.

509 20. Knogler, L.D., and Drapeau, P. (2014). Sensory gating of an embryonic zebrafish  
510 interneuron during spontaneous motor behaviors. *Front. Neural Circuits* 8, 121.

511 21. Wells, S., Nornes, S., and Lardelli, M. (2011). Transgenic zebrafish recapitulating

512 *tbx16* gene early developmental expression. PLoS One 6, e21559.

513 22. Warp, E., Agarwal, G., Wyart, C., Friedmann, D., Oldfield, C.S., Conner, A., Del  
514 Bene, F., Arrenberg, A.B., Baier, H., and Isacoff, E.Y. (2012). Emergence of patterned  
515 activity in the developing zebrafish spinal cord. Curr. Biol. 22, 93-102.

516 23. Kucenas, S., Soto, F., Cox, J.A., and Voigt, M.M. (2006). Selective labeling of  
517 central and peripheral sensory neurons in the developing zebrafish using P2X(3)  
518 receptor subunit transgenes. Neuroscience 138, 641-652.

519 24. Brustein, E., and Drapeau, P. (2005). Serotonergic modulation of chloride  
520 homeostasis during maturation of the locomotor network in zebrafish. J. Neurosci.  
521 25, 10607-10616.

522 25. Freund, T.F., and Buzsaki, G. (1996). Interneurons of the hippocampus.  
523 Hippocampus 6, 347-470.

524 26. Jonas, P., Bischofberger, J., Fricker, D., and Miles, R. (2004). Interneuron Diversity  
525 series: Fast in, fast out--temporal and spatial signal processing in hippocampal  
526 interneurons. Trends in Neurosciences 27, 30-40.

527 27. Freund, T.F., and Katona, I. (2007). Perisomatic inhibition. Neuron 56, 33-42.

528 28. Huang, Z.J., Di Cristo, G., and Ango, F. (2007). Development of GABA innervation  
529 in the cerebral and cerebellar cortices. Nature Reviews Neuroscience 8, 673-686.

530 29. Mirat, O., Sternberg, J.R., Severi, K.E., and Wyart, C. (2013). ZebraZoom: an  
531 automated program for high-throughput behavioral analysis and categorization.  
532 Frontiers in Neural Circuits 7, 107.

533 30. Dale, N., Roberts, A., Ottersen, O.P., and Storm-Mathisen, J. (1987a). The  
534 development of a population of spinal cord neurons and their axonal projections  
535 revealed by GABA immunocytochemistry in frog embryos. Proc. R. Soc. Lond. B. Biol.  
536 Sci. 232, 205-215.

- 537 31. Dale, N., Roberts, A., Ottersen, O.P., and Storm-Mathisen, J. (1987b). The  
538 morphology and distribution of 'Kolmer-Agduhr cells', a class of cerebrospinal-fluid-  
539 contacting neurons revealed in the frog embryo spinal cord by GABA  
540 immunocytochemistry. *Proc. R. Soc. Lond. B. Biol. Sci.* 232, 193-203.
- 541 32. Christenson, J., Alford, S., Grillner, S., and Hokfelt, T. (1991). Co-localized GABA  
542 and somatostatin use different ionic mechanisms to hyperpolarize target neurons in  
543 the lamprey spinal cord. *Neurosci. Lett.* 134, 93-97.
- 544 33. Jalalvand, E., Robertson, B., Wallen, P., Hill, R.H., and Grillner, S. (2014). Laterally  
545 projecting cerebrospinal fluid-contacting cells in the lamprey spinal cord are of two  
546 distinct types. *J. Comp. Neurol.* 522, 1753-1768.
- 547 34. Nair, A., Azatian, G., and McHenry, M.J. (2015). The kinematics of directional  
548 control in the fast start of zebrafish larvae. *The Journal of Experimental Biology* 218,  
549 3996-4004.
- 550 35. Roberts, A., Hill, N.A., and Hicks, R. (2000). Simple mechanisms organise  
551 orientation of escape swimming in embryos and hatchling tadpoles of *Xenopus*  
552 *laevis*. *The Journal of Experimental Biology* 203, 1869-1885.
- 553 36. Deliagina, T.G., Beloozerova, I.N., Orlovsky, G.N., and Zelenin, P.V. (2014).  
554 Contribution of supraspinal systems to generation of automatic postural responses.  
555 *Frontiers in Integrative Neuroscience* 8, 76.
- 556 37. Necker, R. (2006). Specializations in the lumbosacral vertebral canal and spinal  
557 cord of birds: evidence of a function as a sense organ which is involved in the  
558 control of walking. *Journal of Comparative Physiology A, Neuroethology, sensory,*  
559 *neural, and behavioral physiology* 192, 439-448.39.
- 560 38. Meyer, M.P., and Smith, S.J. (2006). Evidence from in vivo imaging that  
561 synaptogenesis guides the growth and branching of axonal arbors by two distinct  
562 mechanisms. *J. Neurosci.* 26, 3604-3614.

39. Wen, H., and Brehm, P. (2005). Paired motor neuron-muscle recordings in zebrafish test the receptor blockade model for shaping synaptic current. *J. Neurosci.* 25, 8104-8111.

40. Zhu, P., Fajardo, O., Shum, J., Zhang Scharer, Y.P., and Friedrich, R.W. (2012). High-resolution optical control of spatiotemporal neuronal activity patterns in zebrafish using a digital micromirror device. *Nat. Protoc.* 7, 1410-1425.

## Figure Legends

### Figure 1 | CSF-cNs specifically innervate the CaP primary motor neuron

(A) Z projection stack showing a single ventral CSF-cN in a *Tg(pkcd2l1:gal4;UAS:ChR2-mCherry)* double transgenic larva at 3 days post fertilization (dpf). Top right: dorsal, ventral, rostral and caudal orientation indicated by the cross. Central canal location indicated by blue dashed lines.

(B) CSF-cN axons and varicosities in the 3dpf *Tg(pkcd2l1:gal4;UAS:ChR2-mCherry)* transgenic larva surround a dorsal cell body.

(C) Labeling of putative presynaptic boutons originating from a single CSF-cN (arrow) expressing Synaptophysin-GFP in a 4 dpf *Tg(pkcd2l1:gal4;UAS:ChR2-mCherry)* transgenic larva after injection of the construct *UAS:Synaptophysin-GFP*.

(D) Schematic of the experimental paradigm used for ChR2-mediated mapping of connectivity illustrates: top, a CSF-cN expressing ChR2-mCherry (green) illuminated by a short pulse of light and the whole cell patch clamp recording of the target neuron with a pipette containing the Alexa dye to confirm the nature of the cell type; bottom: a 5 ms light pulse is sufficient to induce a single spike reliably in CSF-cNs (see [5]) and a subsequent IPSC recorded in the target neuron.

(E) Z projection stack showing a CaP motor neuron filled with the Alexa dye (magenta) innervated by a single CSF-cN (green) in a 4 dpf

589 *Tg(pkcd2l1:gal4;UAS:ChR2-mCherry)* transgenic larva with sparse expression of  
590 ChR2. Boxed region shows a widefield image with the CaP cell body contacted by  
591 the axonal projection of the labeled CSF-cN. Arrows indicate the dorsal projections  
592 that surround the soma of the CaP motor neuron recorded and filled as well as  
593 another putative CaP motor neuron in the adjacent caudal segment.

594 (F) Current clamp recording of a typical CaP motor neuron showing phasic action  
595 potential firing in response to current injection (steps of 20 pA from -50 pA to +90  
596 pA).

597 (G) Voltage clamp recording from a CaP motor neuron ( $V_m = -65$  mV) showing  
598 evoked IPSCs following 5 ms light pulses before (black trace, average of 10 trials)  
599 and after 10  $\mu$ M gabazine treatment (red trace, average of 10 trials).

600 (H) Summary data showing the IPSCs are abolished by gabazine. Each experiment  
601 (grey circle) is the average of ten trials before (Ctl) and after gabazine (Gbz)  
602 treatment (mean amplitude of control IPSC =  $36.2 \pm 24.9$  pA, mean amplitude of  
603 gabazine IPSC =  $5.4 \pm 4.1$  pA,  $n = 5$ ,  $p < 0.0001$ ).

604 (I, J) Voltage steps and corresponding I-V curve indicate that the IPSCs (within the  
605 red dashed box) reverse at  $-53$  mV (red trace in (I) indicates  $-50$  mV), close to the  
606 reversal potential of chloride ( $E_{Cl} = -51$  mV) in our recording conditions ( $n = 6$  cells).

607 (K-N) Distribution of IPSC delay (H, mean =  $6.86 \pm 0.09$  ms), 20-80% rise time (I,  
608 mean =  $0.89 \pm 0.19$  ms), current amplitude (J, mean =  $55.19 \pm 2.34$  pA  
609 corresponding to a conductance of 3.94 nS) and time decay (K, mean  $\tau = 18.04 \pm$   
610  $0.42$  ms) ( $n = 34$  cells, 271 trials).

611 Scale bars are 10  $\mu$ m in 1A-1C and 1E.

## 612 **Figure 2 | Motor neurons other than CaP receive limited CSF-cN input**

613 (A) Motor neurons and CSF-cNs labeled in the *Tg(parg<sup>mnet2</sup>-GFP;*  
614 *pkcd2l1:gal4;UAS:ChR2-mCherry)* transgenic line throughout the rostro-caudal axis

615 (12 axial segments) at 3 dpf. Boxes with magnified images highlight extensive  
616 innervation of large dorsal CaP primary motor neurons (labeled C). However, other  
617 (non-CaP) primary motor neurons (indicated by arrows) and secondary motor  
618 neurons (indicated by arrowheads) do not exhibit the same extensive perisomatic  
619 innervation. Scale bars are 20  $\mu\text{m}$  (2A, top) and 10  $\mu\text{m}$  (2A, magnified boxes).

620 (B1-B3) Examples of whole cell recordings from non-CaP primary motor neurons  
621 showing three types of post-synaptic responses observed. (B1) Upper panel, current  
622 clamp recording of a primary motor neuron showing a single action potential in  
623 response to current injection (steps of 40 pA from -50 pA to +70 pA). Lower panel,  
624 voltage clamp recording from the same primary motor neuron ( $V_m = -65$  mV)  
625 showing evoked IPSCs following 5 ms light pulses (black trace is the average of 10  
626 trials shown in grey). (B2) Upper panel, current clamp recording of a primary motor  
627 neuron showing tonic action potentials in response to current injection (steps of 40  
628 pA from -50 pA to +150 pA). Lower panel, voltage clamp recording from the same  
629 primary motor neuron ( $V_m = -65$  mV) showing small evoked IPSCs following 5 ms  
630 light pulses (black trace is the average of 10 trials shown in grey). (B3) Upper panel,  
631 current clamp recording of a primary motor neuron showing a single action potential  
632 in response to current injection (steps of 40 pA from -30 pA to +130 pA). Lower  
633 panel, voltage clamp recording from the same primary motor neuron ( $V_m = -65$  mV)  
634 showing no IPSCs following 5 ms light pulses (black trace is the average of 10 trials  
635 shown in grey).

636 (C) Histogram of IPSC current amplitudes from non-CaP primary motor neurons  
637 (mean =  $1.78 \pm 0.42$  pA,  $n = 17$  cells, 170 trials).

638 (D) Current clamp recording of a secondary motor neuron showing bursts of action  
639 potentials in response to current injection (steps of 20 pA from -30 pA to +30 pA).

640 (E) Example voltage clamp recordings from secondary motor neurons ( $V_m = -65$  mV)  
641 showing no IPSCs following 5 ms light pulses (black trace is the average of 10 trials  
642 shown in grey). IPSCs in secondary motor neurons were never observed following  
643 CSF-cN stimulation ( $n = 10$ ).

**Figure 3 | CSF-cNs innervate CoPA glutamatergic sensory interneurons**

(A1-A4) Z projection stack showing CoPA sensory interneurons expressing GFP (magenta) innervated by CSF-cNs (green) in *Tg(pkd2l1:gal4;UAS:ChR2-mCherry;tbx16:GFP)* transgenic larvae. Note the varicosities (arrows) from CSF-cNs onto CoPA soma (A1, A2), initial segment (A2, A3) and sometimes dendrites (A3, A4). Scale bars are 10  $\mu$ m.

(B) Current clamp recording of a typical CoPA interneuron showing sparse action potential firing in response to current injections (steps are 20 pA from -50 pA to +150 pA).

(C) Voltage clamp recording from a CoPA interneuron ( $V_m = -65$  mV) showing an evoked IPSC following a 5 ms light pulse (black trace, average of 10 trials).

(D-G) Distribution of IPSC delay (D, mean =  $7.73 \pm 0.15$  ms), 20-80% rise time (E, mean =  $0.88 \pm 0.08$  ms), amplitude (F, mean =  $146.83 \pm 16.75$  pA corresponding to a conductance of 10.49 nS) and time decay  $\tau$  (G, mean =  $18.16 \pm 1.22$  ms) (n = 8 cells, 64 trials).

(H) Cumulative probability plot of IPSC amplitudes for CaP motor neurons (blue, n = 271) and CoPA interneurons (red, n = 64).

**Figure 4 | 2D Light patterning at the single cell resolution reveals convergence of inputs from CSF-cNs onto their targets**

(A) Schematic of the Digital Mirror Device (DMD) setup showing the light path. A beamsplitter (1) was attached to the epi-port of an upright microscope in order to combine light from the epifluorescence light source via fiber optic (2) and the light from the DMD. The patterned light from the DMD was relayed into the epifluorescence light path via a telescope (3). A white Light Emitting Device (LED) (4) providing the light for patterned illumination was directed via a total internal reflection prism (5) to the DMD (6).

671 (B, C) Physiological responses to either full field illumination (B) or a small spot on an  
672 individual CSF-cN (C). Top: Fluorescent image of multiple CSF-cNs from the  
673 *Tg(pkcd2l1:gal4;UAS:ChR2-mCherry)* transgenic line with all (B) or a subset of the  
674 central mirrors activated (C). Scale bar, 20  $\mu$ M Bottom: IPSCs following a 5 ms light  
675 pulse from either full field (B) or patterned illumination (C). In cases where only one  
676 CSF-cN is connected to the target, the IPSC amplitude evoked by the spot  
677 recapitulates the IPSC amplitude evoked by the full field illumination. Scale bars are  
678 50 ms and 20 pA.

679  
680 (D) Example experiment investigating the connectivity from CSF-cNs (green) to a CaP  
681 motor neuron (magenta) showing multiple CSF-cNs projecting onto the postsynaptic  
682 target. Light was patterned in rectangles (indicated in yellow), which were  
683 sequentially illuminated along the rostro-caudal axis during voltage clamp recording  
684 of the target neuron. Right: voltage clamp traces resulting from the light activation  
685 of the corresponding rectangular region. IPSCs are observed when the light is  
686 patterned onto a subset of CSF-cNs (yellow stars). White dashed lines indicate  
687 segment boundaries. Scale bars are 50  $\mu$ m for the image and 10 ms and 50 pA for  
688 the electrophysiological traces.

689 (E) Quantification of the IPSC amplitude for CaP (blue circles) and CoPA (red circles)  
690 as a function of the number of segments between a CSF-cN and its target. Mean  
691 IPSC amplitude for CaP and CoPA combined are plotted for each segment (white  
692 boxes).

693 (F) Convergence of CSF-cNs onto a CaP motor neuron. Image of CSF-cNs expressing  
694 ChR2-mCherry (green) and the target CaP motor neuron filled with Alexa dye  
695 (magenta). IPSCs in response to either full field or patterned illumination show that  
696 cells "4" and "6" converge on the CaP motor neuron target.

697 (G, H) Examples of identified connections from CSF-cNs onto CaP motor neurons (G)  
698 and CoPA neurons (H) in three different larvae. Arrows indicate patched target cell  
699 body. Yellow circles show connected CSF-cNs. Scale bars are 50  $\mu$ m.



**Figure 5 | CSF-cN local innervation onto the escape circuit is restricted to excitatory interneurons and motor neurons**

(A) Z projection stack of CoLo glycinergic premotor interneurons expressing GFP (magenta) and CSF-cNs (green) in a *Tg(pkcd2l1:gal4;UAS:ChR2-mCherry; Tol-056-GFP)* transgenic larva at 3 dpf. Arrows indicate CoLo cell bodies. Scale bar is 10  $\mu$ m.

(B) Current clamp recording showing the typical firing pattern of a CoLo neuron with a single weak action potential in response to current injection (steps of 20 pA from -30 pA to +370 pA).

(C). CSF-cN stimulation elicited by a 5 ms light pulse fails to induce a IPSCs in CoLos. Example voltage clamp recordings from three CoLos ( $V_m = -65$  mV) showing no IPSCs following 5 ms light pulses (black trace is the average of 10 trials shown in grey). IPSCs in CoLo were never observed following CSF-cN stimulation (n = 13 cells).

(D) Z projection stack showing Rohon-Beard neurons expressing GFP (magenta) and CSF-cNs (green) in a *Tg(pkcd2l1:gal4;UAS:ChR2-mCherry; p2rx3.2:GFP)* transgenic larva at 3 dpf. Note the axonal projections of CSF-cNs do not reach Rohon-Beard somas or axons. Scale bar is 10  $\mu$ m.

(E) Current clamp recording showing the typical firing pattern of a Rohon-Beard neuron with a single weak action potential in response to current injection (steps of 20 pA from -30 pA to +170 pA).

(F) CSF-cN stimulation elicited by a 5 ms light pulse fails to induce an IPSC in Rohon-Beard neurons. Example voltage clamp recordings from three Rohon-Beard neurons ( $V_m = -65$  mV) showing no IPSCs following 5 ms light pulses (black trace is the average of 10 trials shown in grey). IPSCs in Rohon-Beard neurons were never observed following CSF-cN stimulation (n = 10 cells).

**Figure 6 | Stimulation of CSF-cNs at moderate frequencies results in short-term synaptic depression in CaP motor neurons and CoPA interneurons**

(A1, A2) Typical examples of IPSCs (grey) recorded from CaP (A) and CoPA (B) at 0.2 Hz. Average of 10 trials in black. Note the absence of failure and the large IPSC amplitude.

(A3) Stimulation at 0.2 Hz induced moderate short term depression in CaP (blue circles, t-test for the difference between the 1<sup>st</sup> and the 10<sup>th</sup> light pulse  $p = 0.036$ ,  $n = 7$ ) and no depression for CoPA (red triangles,  $p = 0.48$ ,  $n = 5$ ).

(B1, B2) Typical examples of IPSCs recorded from CaP (B1) and CoPA (B2) at 1 Hz. Trace is an average of 10 trials. Note the absence of failure of the IPSC.

(B3) Trains of stimuli at 1 Hz induce small but significant short term depression (23% for CaP, blue circles,  $p = 0.037$ ,  $n = 7$  and 41% for CoPA, red triangles,  $p = 0.030$ ,  $n = 5$ ).

(C1, C2) Typical examples of IPSCs recorded from CaP (C1) and CoPA (C2) at 10 Hz. Trace is an average of 10 trials. Note the absence of failure and the promptly decreasing amplitude of the IPSC.

(C3) Trains of stimuli at 10 Hz induce large, significant short term depression (57% for CaP, blue circles,  $p = 0.00002$ ,  $n = 7$  and 75% for CoPA, red triangles,  $p = 0.00009$ ,  $n = 5$ ).

(D1, D2) Typical examples of IPSCs recorded from CaP (D1) and CoPA (D2) at 20 Hz. Trace is an average of 10 trials. Note the absence of failure and the promptly decreasing amplitude of the IPSC.

(D3) Trains of stimuli at 20 Hz induce large, significant short term depression (68% for CaP, blue circles,  $p = 0.000008$ ,  $n = 7$  and 81% for CoPA, red triangles,  $p = 0.00005$ ,  $n = 5$ ).

**Figure 7 | Silencing CSF-cNs induces a defect in balance during fast swimming**

(A) A voltage step (+180 mV for 100 ms from a holding potential of -65 mV) in cell-attached mode leads to high frequency CaP motor neuron spiking in the control condition.

(B) Typical trial showing that in a *Tg(pkcd2l1:gal4 ; UAS:ChR2-mCherry)* transgenic larva a 5 ms light pulse applied during the voltage step leads to the prompt silencing of the CaP motor neuron for approximately 20 ms.

(C) Raster plot of CaP spiking without (top trace) and with (bottom 10 traces) optogenetic stimulation of CSF-cNs. Repetition of 10 sequential trials confirms the robust effect of silencing CaP firing. The duration of silencing tended to increase during sequential trials.

(D) Maximum interspike interval (ISI) was quantified for 5 spikes prior to the light pulse and 5 spikes following the light pulse. All cells showed silencing following the 5 ms light pulse illustrated by an increase in ISI ( $9.10 \text{ ms} \pm 3.04 \text{ ms}$  before and  $26.69 \text{ ms} \pm 10.55 \text{ ms}$  after light pulse,  $n = 4$ , paired t-test:  $p = 0.02$ ).

(E) Sample sequence of images acquired with a high speed camera during acoustically evoked escaped responses for *Tg(pkcd2l1:gal4 ; UAS:BotxBLC-GFP)* transgenic larvae and control siblings. Magnified images (5 panels on the left) demonstrate the rolling phenotype when CSF-cNs are genetically targeted with BotxBLC-GFP+ to silence GABA release (scale bars are 1 mm). Z-stack of the entire escape response sequence for BotxBLC-GFP+ and control siblings (panels on right, scale bars are 2mm).

(F) Calculated roll ratio for *Tg(pkcd2l1:gal4 ; UAS:BotxBLC-GFP)* transgenic larvae and control siblings ( $n = 148$  fish for each genotype). BotxBLC-GFP+ fish were significantly more likely to tip over and roll during the escape response than the control siblings ( $p < 0.001$ ).

Figure 1

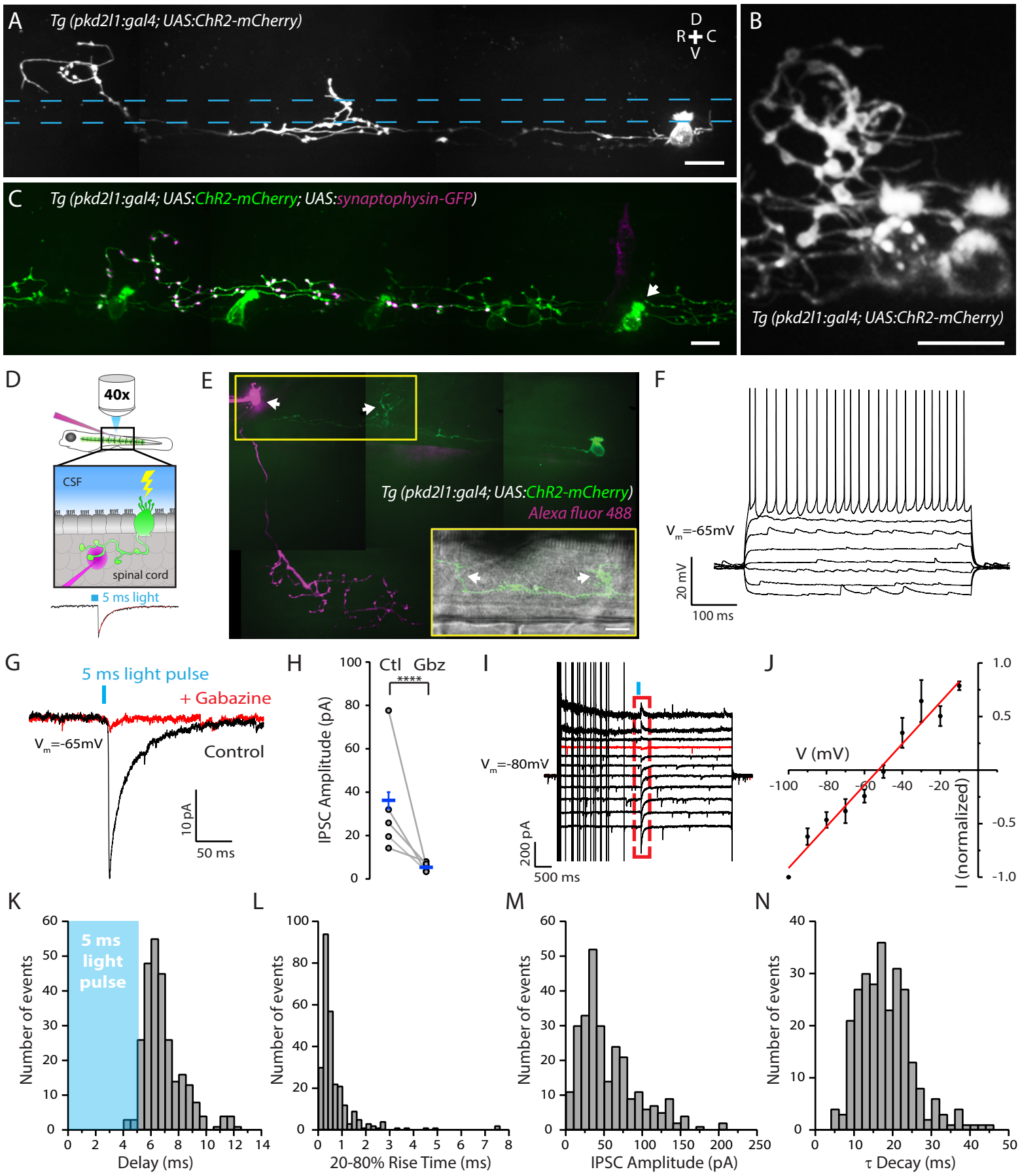


Figure 2

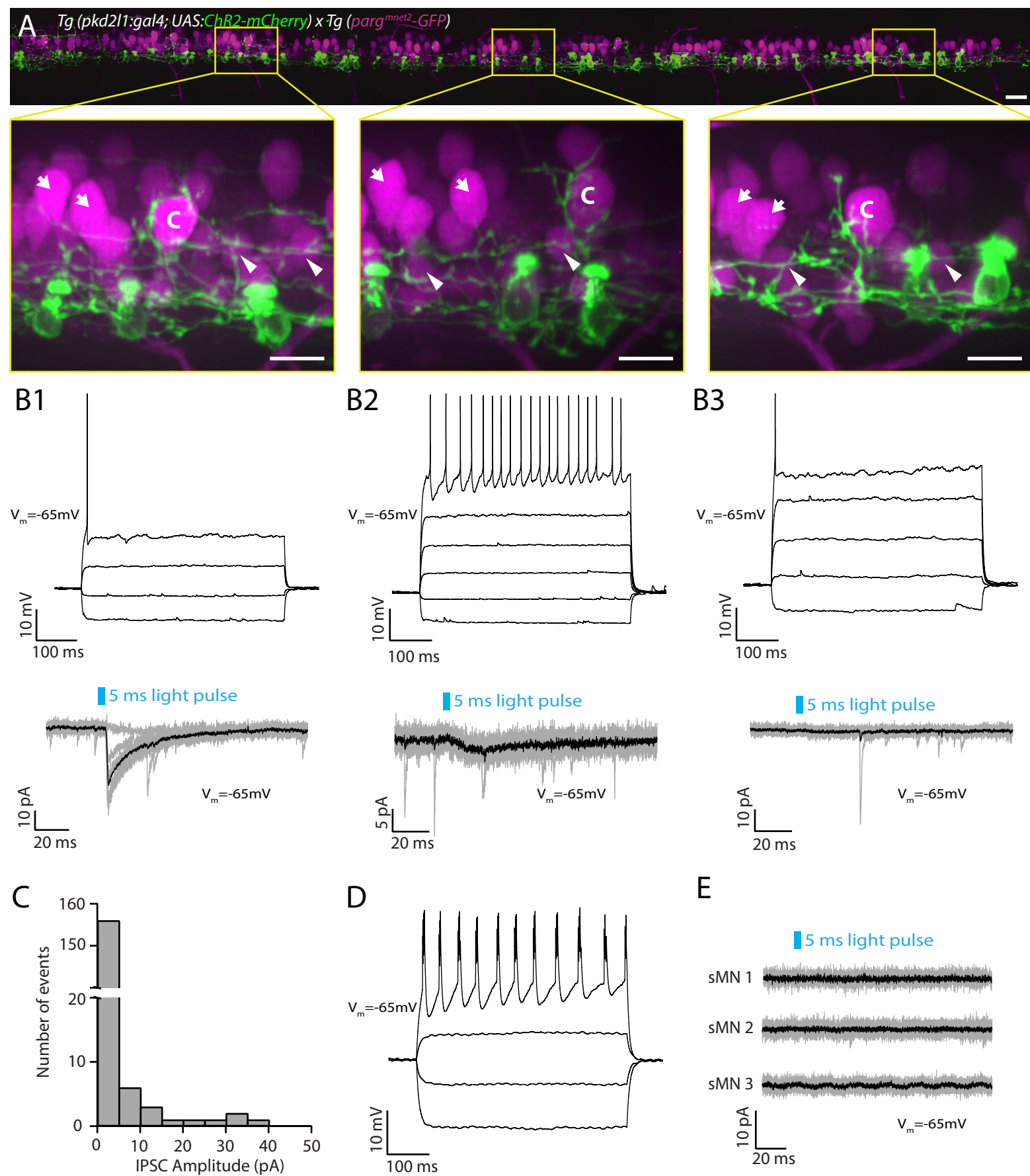




Figure 3

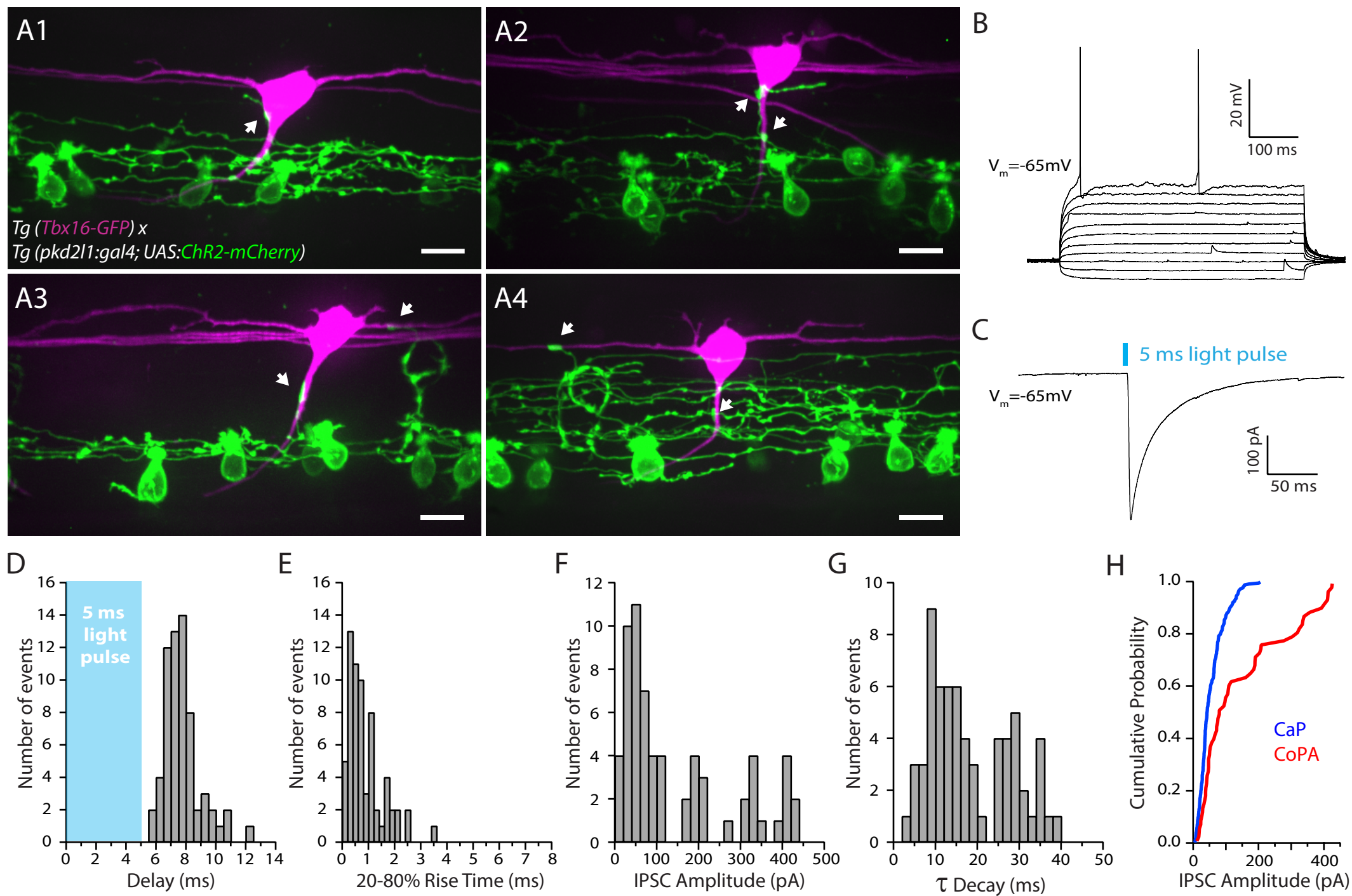
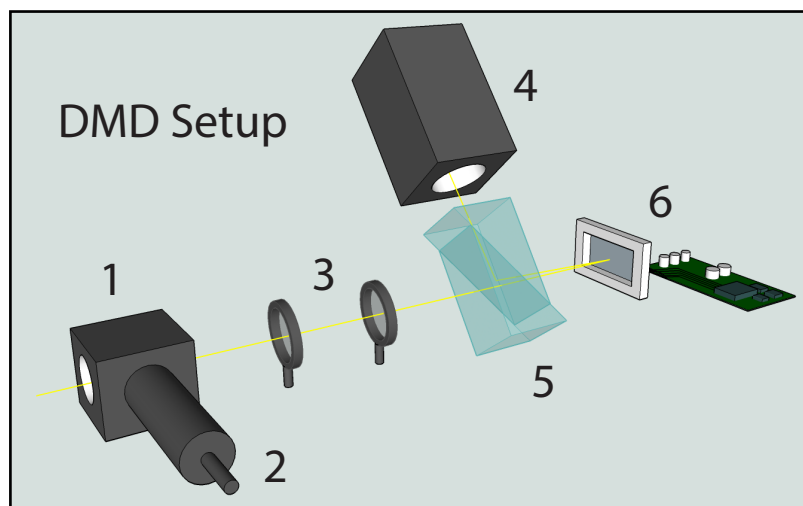
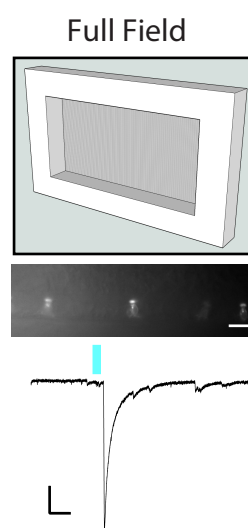


Figure 4

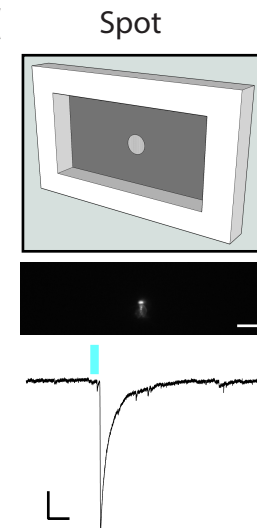
A



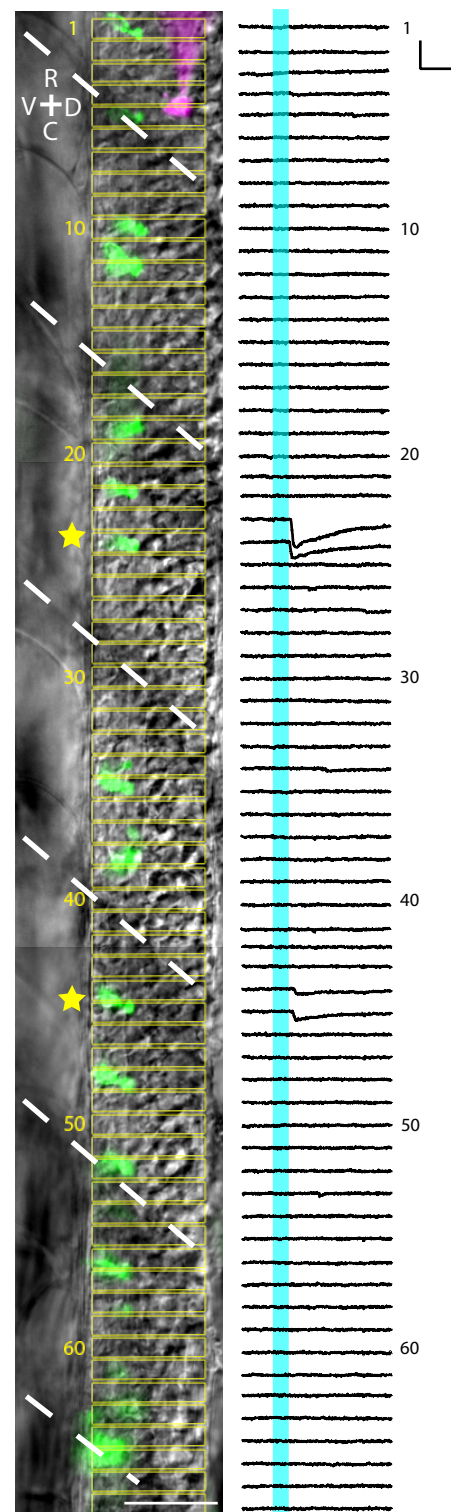
B



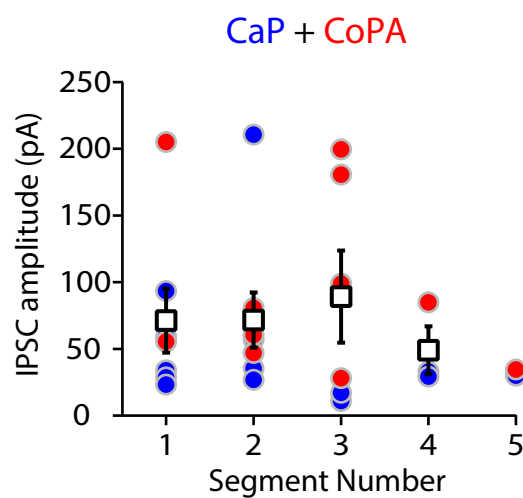
C



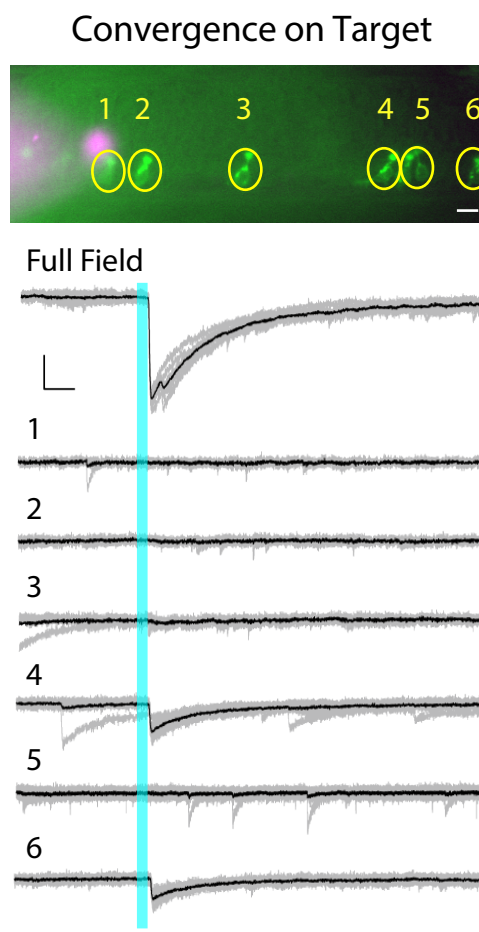
D



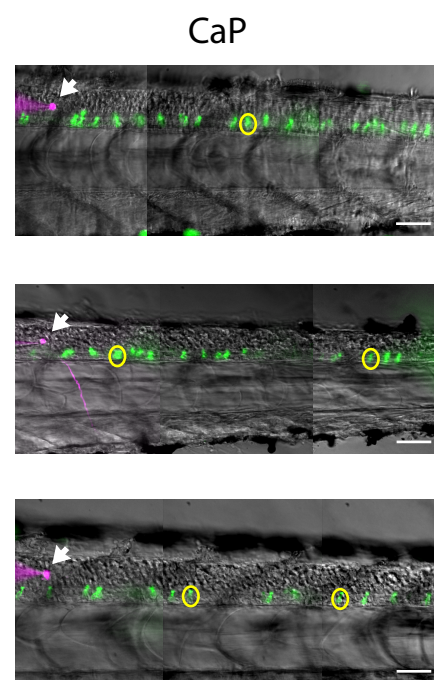
E



F



G



H

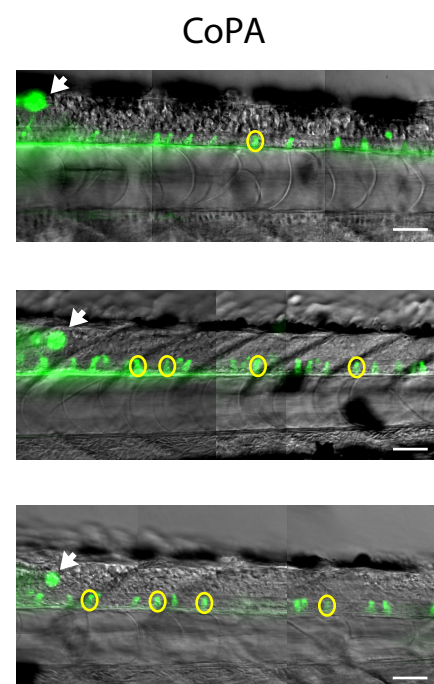


Figure 5

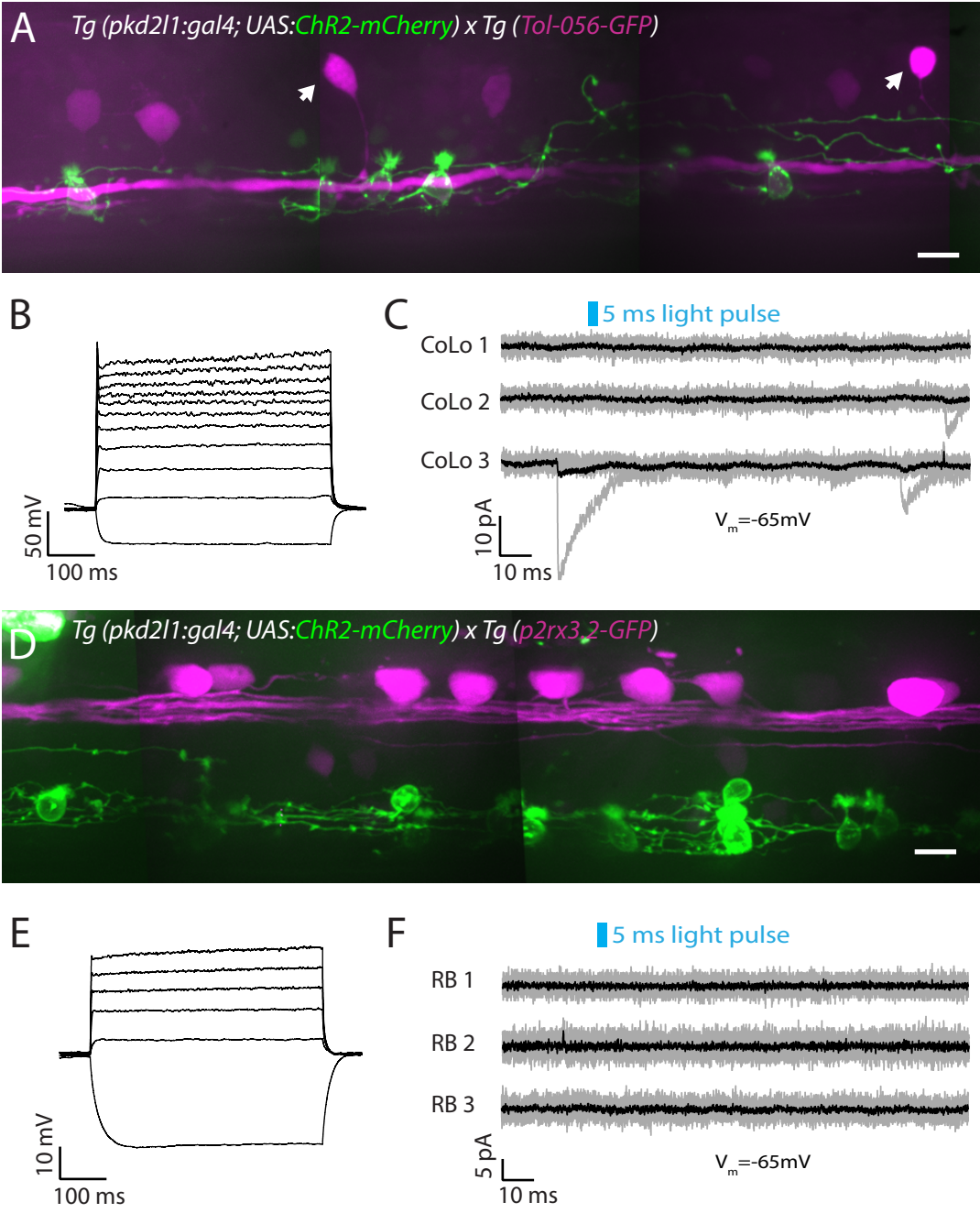




Figure 6

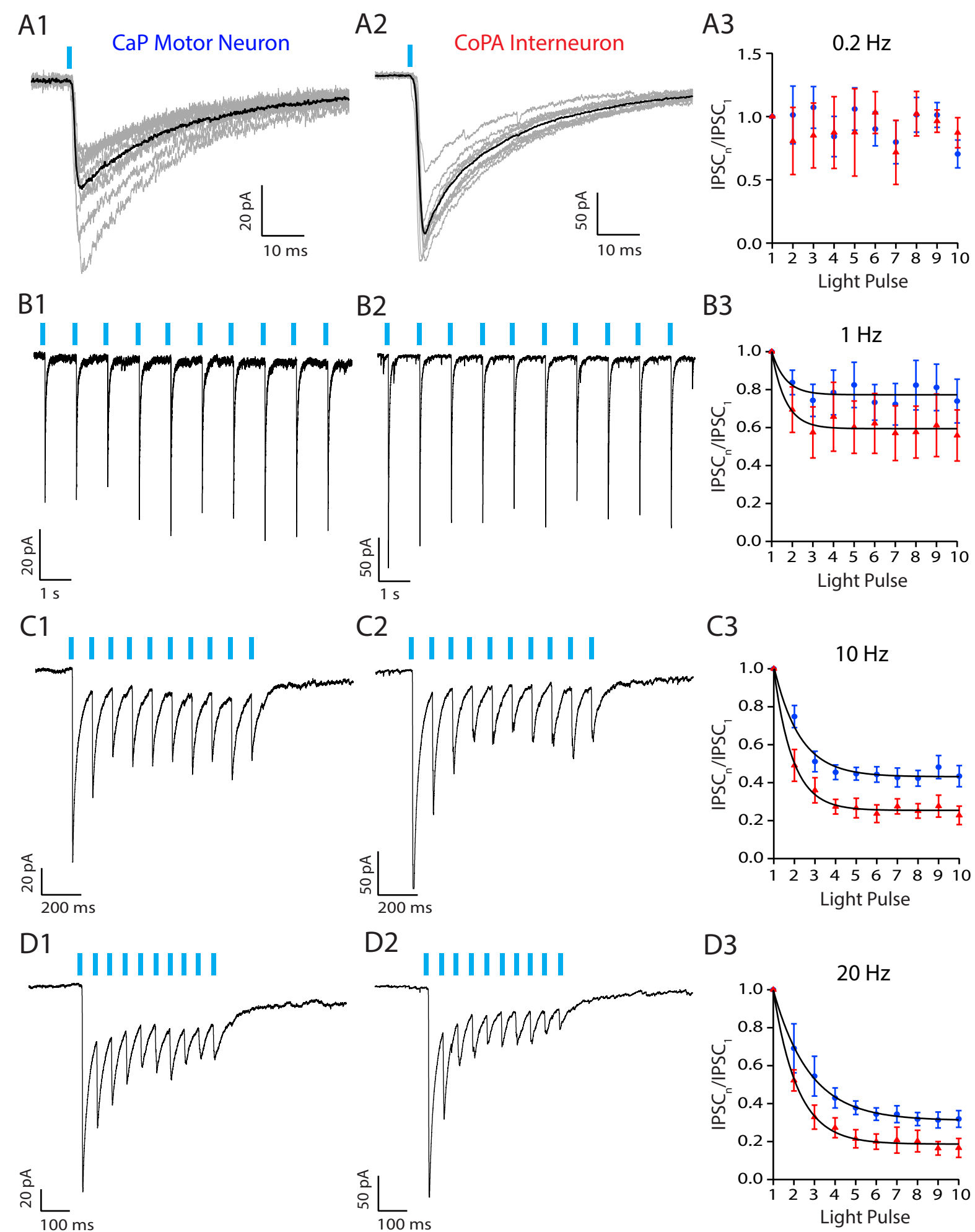
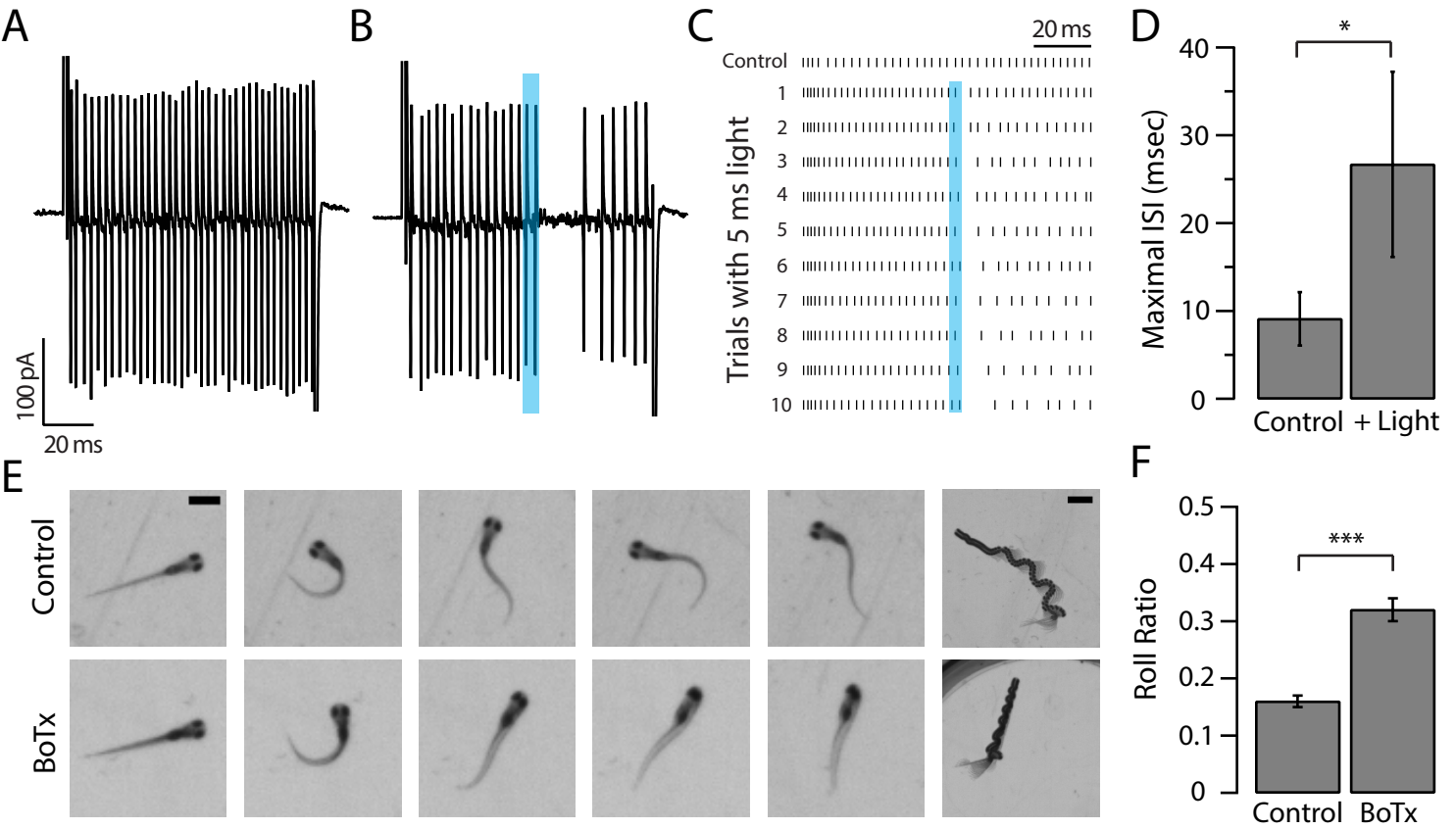
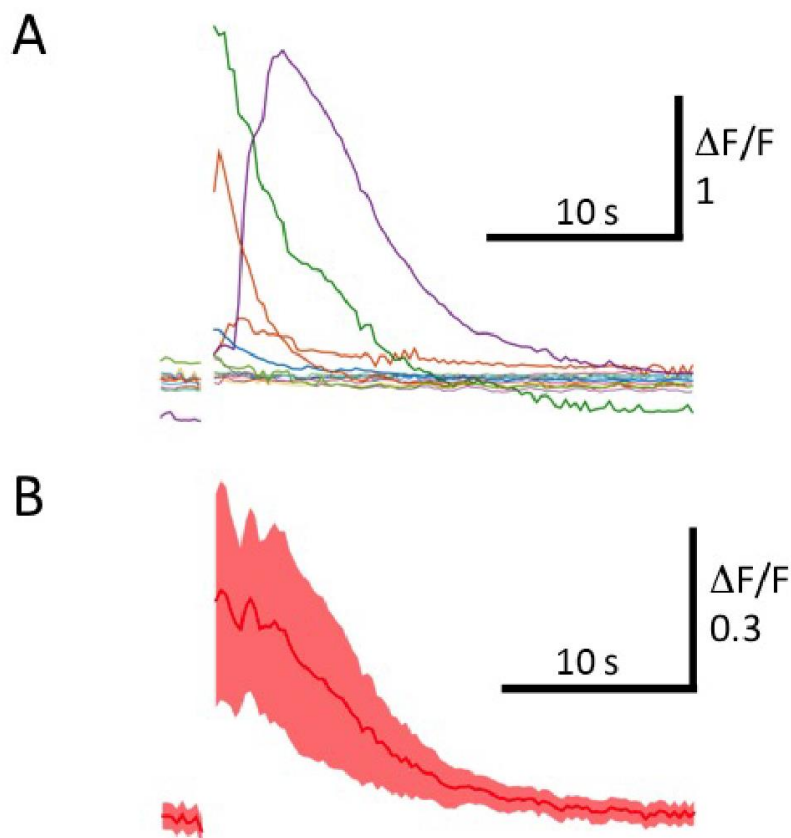


Figure 7



# Supplemental information Hubbard et al.



**Figure S1. Related to Figure 7. Calcium response of ventral CSF-cNs to longitudinal contractions.**

(A) Single traces of  $\text{Ca}^{2+}$  activity in ventral CSF-cNs in response to spontaneous contractions of 5-7 dpf *Tg(pkcd211:gal4; UAS:GCaMP3; UAS:mCherry)* larvae embedded on their side. Visible is the strong response of several cells due to the muscle contraction.  $N = 13$  cells from 3 fish. (B) Average response of the data presented in A. Shaded area designates the S.E.M.

## **Movie S1. Related to Figure 7. Spontaneous muscle contractions activate CSF-cNs.**

Example movie of calcium signals from GCaMP3 fluorescence in CSF-cNs during spontaneous muscle contractions. Images were acquired at 4 Hz and the movie is compressed to 60 frames per second (fps).

## **Movie S2. Related to Figure 7. WT escape response.**

Example movie of an acoustically-induced escape response in a control animal. The larva swims upright without rolling over in most cases. Images were acquired at 650 Hz and the movie is shown at 15 fps. Scale bar is 2 mm.

## **Movie S3. Related to Figure 7. BoTx escape response.**

Example movie of an acoustically induced escape response in a BoTxBLC+ animal. The larva is initially upright and rolls over during the escape. Note that the swim bladder is initially down, but our camera captures an inverted image of the animal. Images were acquired at 650 Hz and the movie is shown at 15 fps. Scale bar is 2 mm.

**Table S1. Summary of stable transgenic lines used in this study**

<b>Table 1 : Transgenic lines</b>			
Name	Other Name	Labelling in the spinal cord	Original publication
<i>Tg(pkd2l1:gal4)icm10</i>	-	CSF-cNs	Fidelin et al., 2015 [S1]
<i>Tg(UAS:ChR2-mCherry)</i>	<i>Tg(UAS:ChR2H134R-mCherry)</i>	-	Schoonheim et al., 2010 [S2]
<i>Tg(parg:GFP)mnet2</i>	-	Motor Neurons	Balciunas et al., 2004 [S3]
<i>Tg(Tol56:GFP)</i>	Tol56	CoLo	Satou et al., 2009 [S4]
<i>Tg(tbx16:GFP)812C</i>	812C	CoPA	Wells et al., 2011 [S5]
<i>Tg(p2x3.2::eGFP<sup>GR</sup>)</i>	<i>Tg(p2rx3.2<sup>GR</sup>)</i>	Rohon Beard neurons	Kucenas et al., 2006 [S6]
<i>Tg(UAS:BoTxBLC-GFP)</i>	<i>Tg(UAS:BoTxBLC-GFP)</i>	-	Auer et al., eLife 2015 [S7] ; Böhm et al., Nature Communications 2016 [S8] ; Sternberg et al., <i>in press.</i> [S9]
<i>Tg(UAS :GCaMP3)</i>	<i>Tg(UAS :GCaMP3)</i>	-	Warp et al., Curr. Biol. [S10]

## Supplemental Experimental Procedures

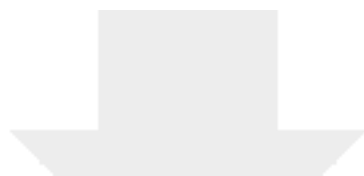
### *In vivo* imaging of calcium

5-7 dpf *Tg(pkd2l1:gal4; UAS:GCaMP3; UAS:mCherry)* were laterally embedded in 1.5% low melting agarose. Images were acquired at 4Hz on a widefield microscope (Axio Examiner D1, Zeiss, Germany). To correct the motion artifact due to muscle contraction, the calcium signal from GCaMP3 fluorescence and the control signal from mCherry fluorescence were recorded simultaneously on two cameras (ImageEM, Hamamatsu, Japan and Stingray F145B, Allied Vision, Germany) using a dual excitation/emission filter set (GFP/DsRed-A-000, Semrock, USA). Images were processed as described in Böhm and Prendergast *et al.*, 2016 and the fluorescence ratio plotted.

## Supplemental References

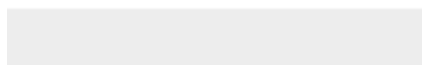
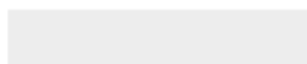
S1. Fidelin, K., Djenoune, L., Stokes, C., Prendergast, A., Gomez, J., Baradel, A., Del Bene, F., Wyart, C. (2015). State-Dependent Modulation of Locomotion by GABAergic Spinal Sensory Neurons. *Curr. Biol.* 25, 3035-47.

- S2. Schoonheim, P. J., Arrenberg, A. B., Del Bene, F., and Baier, H. (2010). Optogenetic localization and genetic perturbation of saccade-generating neurons in zebrafish. *J. Neurosci.* 30, 7111-7120.
- S3. Balciunas, D., Davidson, A.E., Sivasubbu, S., Hermanson, S.B., Welle, Z., and Ekker, S.C. (2004). Enhancer trapping in zebrafish using the Sleeping Beauty transposon. *BMC genomics* 5, 62.
- S4. Satou, C., Kimura, Y., Kohashi, T., Horikawa, K., Takeda, H., Oda, Y., and Higashijima, S. (2009). Functional role of a specialized class of spinal commissural inhibitory neurons during fast escapes in zebrafish. *J. Neurosci.* 29, 6780-6793.
- S5. Wells, S., Nornes, S., and Lardelli, M. (2011). Transgenic zebrafish recapitulating *tbx16* gene early developmental expression. *PLoS One* 6, e21559.
- S6. Kucenas, S., Soto, F., Cox, J.A., and Voigt, M.M. (2006). Selective labeling of central and peripheral sensory neurons in the developing zebrafish using P2X(3) receptor subunit transgenes. *Neuroscience* 138, 641-652.
- S7. Auer, T.O., Xiao, T., Bercier, V., Gebhardt, C., Duroure, K., Condordet, J-P., Wyart, C., Suster, M., Kawakami, K., Wittbrodt, J., Baier, H., and Del Bene, F. (2015). Deletion of a kinesin 1 motor unmasks a mechanism of homeostatic branching control by neurotrophin-3. *eLife* 4, e05061.
- S8. Böhm, U.L., Prendergast, A., Djenoune, L., Nunes Figueiredo, S., Gomez, J., Stokes, C., Kaiser, S., Suster, M., Kawakami, K., Charpentier, M., et al. (2016). CSF-contacting neurons regulate locomotion by relaying mechanical stimuli to spinal circuits. *Nature communications* 7, 10866.
- S9. Sternberg, J.R., Severi, K.E., Fidelin, K., Gomez, J., Ihara, H., Alcheikh, Y., Hubbard, J.M., Kawakami, K., Suster, M., Wyart, C. (2016). Optimization of a neurotoxin to investigate the contribution of excitatory interneurons to speed modulation *in vivo*. *Curr Biol.* (*in press*).
- S10. Warp, E., Agarwal, G., Wyart, C., Friedmann, D., Oldfield, C.S., Conner, A., Del Bene, F., Arrenberg, A.B., Baier, H., Isacoff, E.Y. (2012). Emergence of patterned activity in the developing zebrafish spinal cord. *Curr. Biol.* 22: 93-102.



[Click here to access/download](#)

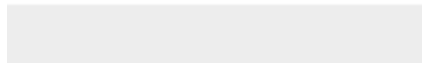
**Supplemental Movies & Spreadsheets**  
Supplemental Video S1.avi





[Click here to access/download](#)

**Supplemental Movies & Spreadsheets**  
Supplemental Video S2.avi





[Click here to access/download](#)

**Supplemental Movies & Spreadsheets**  
Supplemental Video S3.avi

